Field Emission of Carbon Nanotubes from Various Tip Structures

Jisoon Ihm and Seungwu Han

Department of Physics and Center for Theoretical Physics
Seoul National University
Seoul 151-742, Korea
E-mail: nsjisoon@phya.snu.ac.kr

INTRODUCTION

From the beginning of its discovery, the carbon nanotube (CNT) has been regarded as an ideal material to make field emitters because of its unusually high aspect ratio as well as mechanical and chemical stability. Many experiments with singlewall[1,2] and multiwall[3,4,5,6,7] carbon nanotubes have demonstrated a relatively low threshold voltage of the electron emission with little sample degradation. Recently, flat panel displays fabricated with the CNT's as emitters are demonstrated[8]. Furthermore, the advancements in fabrication technology make it possible to generate a self-aligned or a patterned CNT on a glass[9] or a silicon substrate[10], implying that a commercial production of the CNT-based field emission display (FED) may be possible in near future.

In spite of the accumulating experimental data, realistic quantum mechanical calculations on the field emission of the CNT are still scarce. The simplistic view of the CNT as a jellium metallic emitter based on the conventional Fowler-Nordheim theory could not explain the entire range of the I-V data[1,7] and a critical analysis of the electronic structure on a more fundamental level is required. In this study, we perform *ab initio* pseudopotential electronic structure calculations[11,12] with or without applied fields. We focus on the end geometries of the CNT where the electron emission actually occurs and try to find the optimized tip structure for field emission. Some of the results presented here have been submitted for publication elsewhere[13].

MODEL SYSTEM AND COMPUTATIONAL METHOD

We consider various end geometries of the CNT. The side views of the upper part of the (5,5) CNT's are shown in Fig. 1. The bottom (not shown) of the tube body is terminated with hydrogen atoms for computational convenience. We call (a)-(d) as H(hydrogen-attached)-, FC(flat-cut)-, CAP(capped)-, and SC(slant-cut)-CNT, respectively. The H-CNT represents a situation where the dangling bonds are chemically stabilized by ambient hydrogen. In the CAP-CNT model, the tube end is capped with

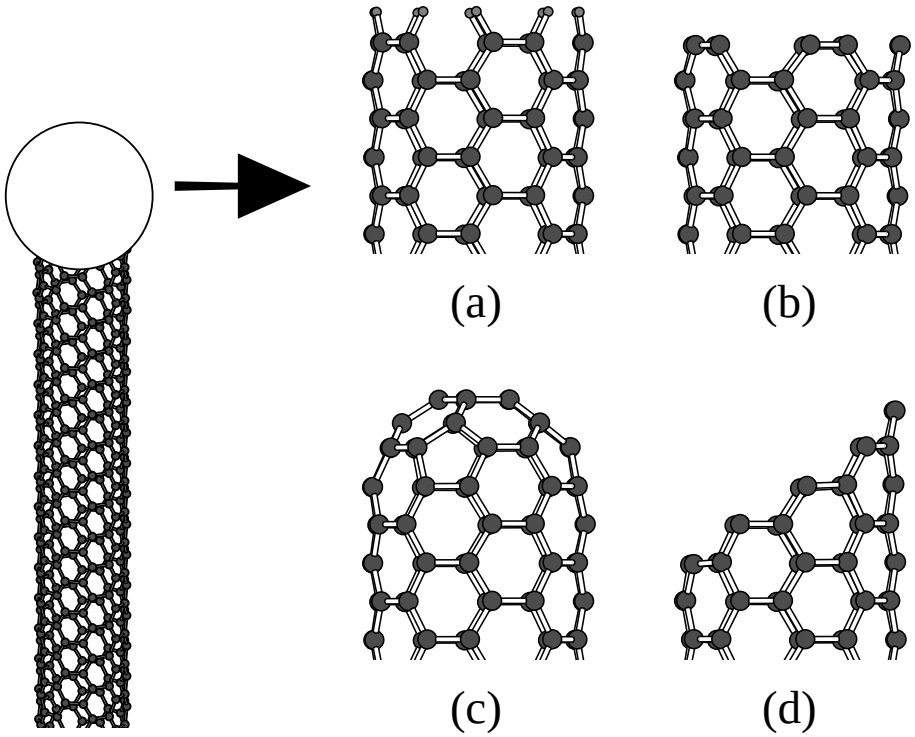

Figure 1. Edge structures studied in this work. (a) H-CNT, (b) FC-CNT, (c) CAP-CNT, and (d) SC-CNT (see text for abbreviations).

a patch (hemisphere) of C_{60} having six pentagons. In the FC-CNT and SC-CNT, on the other hand, dangling bonds remain unsaturated. The model systems are periodically repeated in a tetragonal supercell with the tube axis lying in the z-direction. In order to make the simulation as realistic as possible, various computational schemes are adopted in this study. The plane-wave based calculations have been done mostly for a $\sim 20\mathring{A} \times 20\mathring{A} \times 30\mathring{A}$ unit supercell. To check the convergence of our results for larger systems, we have also used localized basis functions[14] in the *ab initio* pseudopotential calculations and have been able to enlarge the tube size up to four times. The base grid of 60 Ry. is used for the projection of the orbital and wave function. Relaxed geometries are obtained from computationally less demanding tight-binding calculations [15].

ELECTRONIC STRUCTURE OF MODEL SYSTEMS

In Fig. 2, the total density of states (TDOS) around the Fermi level is plotted in solid lines. All systems except the H-CNT have localized states near the nanotube edge. To investigate these localized states more closely, the local density of states (LDOS) around the end region is calculated and shown in dashed lines in Fig. 2(b) and (c). Energy levels of the localized states induced by the topological defects (pentagons) in the CAP-CNT are known to depend on the relative positions between the defects[16,17,18] and the pentagons are assumed to be separated from each other here as found in Ref. 17. In Fig. 2(d), the LDOS of the SC-CNT at the two topmost atoms (the sharp edge) and that at the eight side atoms on the slant-cut cross section are shown in dotted and dashed lines, respectively. Descriptions about different characters of these two will be given in the following section. In the SC-CNT, localized π states predicted for the graphite ribbons[19] are also found, but they are less prominent than the σ-bond-derived

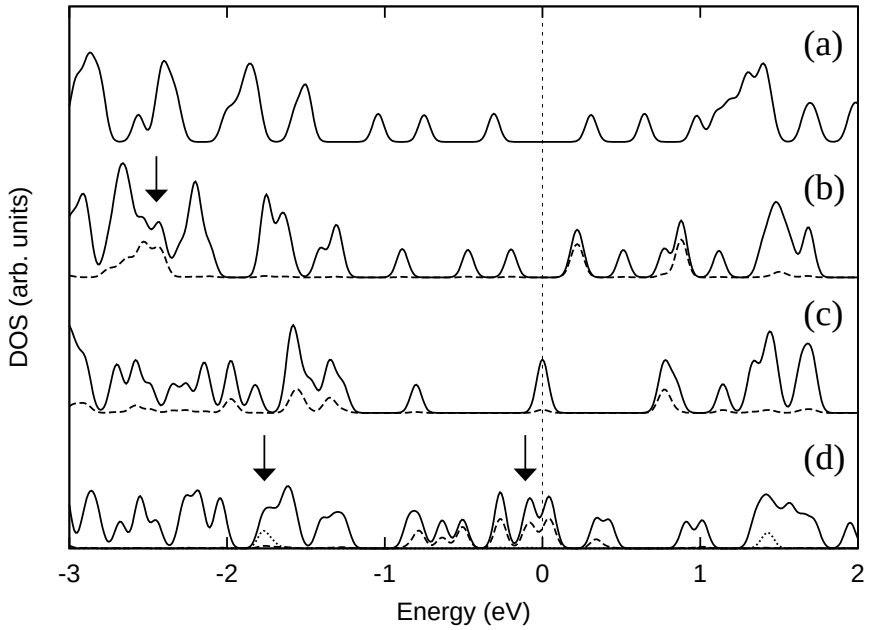

Figure 2. TDOS (solid line) and LDOS (dashed or dotted lines) corresponding to each structure [(a)-(d)] in Fig. 1. The Fermi level is set to zero. The LDOS represents the states localized at the top of the nanotubes in Fig. 1. In (d), the dashed and dotted lines are differentiated as explained in the text.

states and unimportant to field emission.

In Fig. 3(a), we show one of the localized states in the FC-CNT whose energy level is indicated by an arrow in Fig. 2(b). Interestingly, two adjacent dangling bonds join at the backbond position of the original sp^2 configuration. The character of the s-orbital is slightly lost in the sp^2 hybridization. Because of these additional bonds, the C-C bond length in the top layer is $1.27\mathring{A}$ compared with the ideal C-C distance in a perfect nanotube ($1.41\mathring{A}$), corresponding to a strong double bond. Two types of localized states are identified in the SC-CNT model. In Fig. 3(b), the topmost atoms on the armchair-like edge (states at -1.8 eV indicated by an arrow in Fig. 2(d)) show a similar backbonding as in the FC-CNT, while the individual dangling bonds on the side edge (indicated by an arrow at -0.1 eV in Fig. 2(d)) remain unpaired as shown in Fig. 3(c) since they are far apart from each other along the zigzag edge. Since the interaction between them is weak, the energy splitting is small, resulting in a large LDOS at the Fermi level as indicated in dashed line in Fig. 2(d). On the other hand, the energy splitting between the bonding and antibonding states is rather significant ($\sim$3 eV) for the states localized at the armchair edge as shown in two separate dotted curves.

EFFECT OF EXTERNAL FIELDS

A sawtooth-type potential is applied along the CNT axis to simulate a uniform external electric field in the supercell geometry. In the experimental situation, the applied field strength is usually a few V/μm and the length of the CNT is a few μm, resulting in $\sim$ 10 V difference in the applied potential between the tube ends. It has

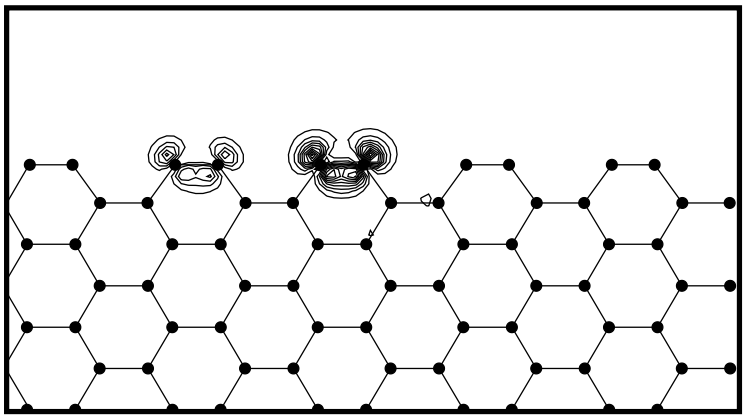

(a)

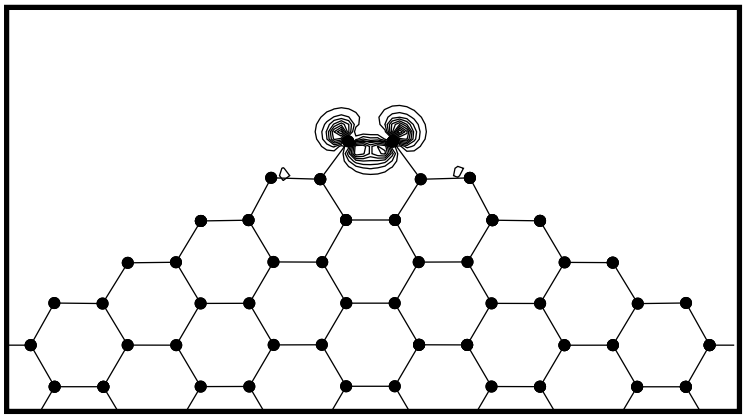

(b)

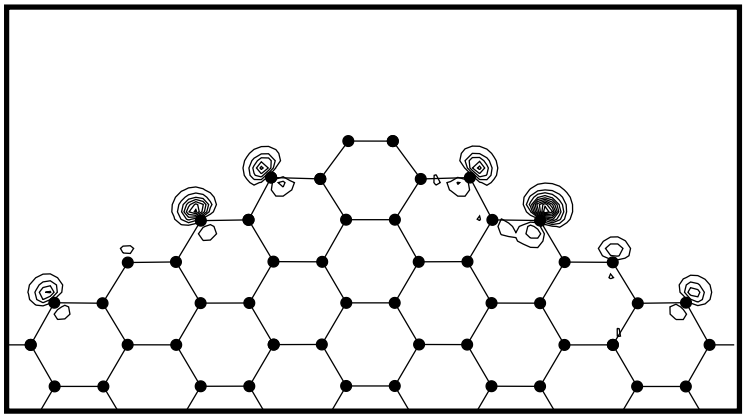

(c)

Figure 3. Electron density of the localized states whose energy levels are indicated by arrows in Fig. 2(b) and (d). (a) is the localized state of the FC-CNT at -2.6 eV and (b) and (c) are the localized states of the SC-CNT at -1.8 eV and -0.1 eV, respectively. The electron density is evaluated on the nanotube surfaces and the contour interval is 0.08 $e/\mathring{A}^3$.

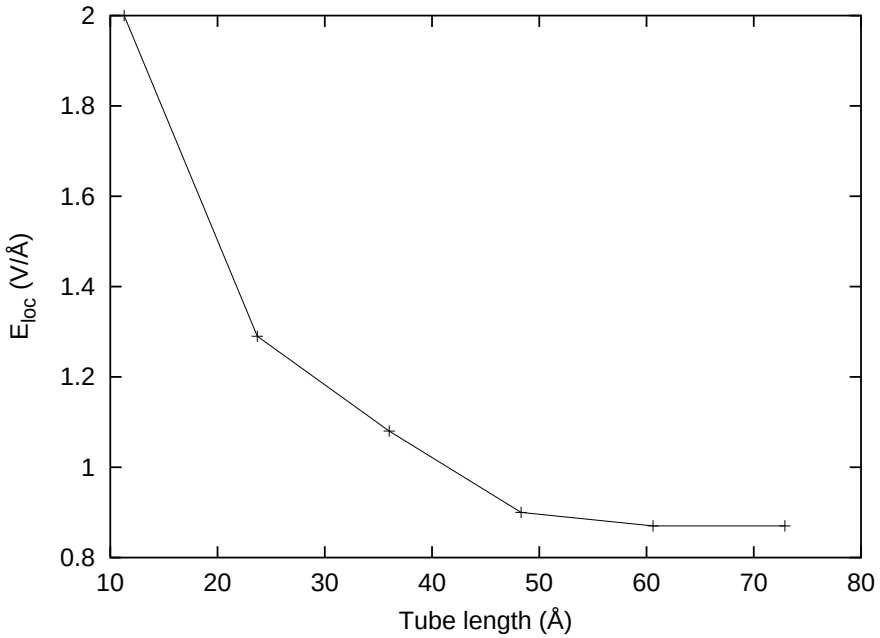

Figure 4. Averaged local field within 3 $\mathring{A}$ outside the tip as a function of the tube length for a CAP-CNT. The applied field is varied so that its product with the tube length is fixed at 10 V.

been well established that the field emission typically occurs when the actual field at the tip is $\sim$ 0.5 V/$\mathring{A}$, corresponding to a field enhancement factor of $\sim$ 1000 in the present experimental situation. Since the system size is severely limited in the *ab initio* calculation, it is a serious issue whether one can mimic the realistic situation and extract meaningful information on the field emission through the *ab initio* calculation for small-size tubes. After many different calculations, we find the following trends as shown in Fig. 4. We apply a uniform field across the supercell such that the potential difference across the tube (i.e., between the two tube ends) is fixed at 10 V for each case. For instance, for 23.7, 48.3, and 72.9 $\mathring{A}$ tubes, the applied field strengths are 0.42, 0.21, and 0.14 V/$\mathring{A}$, respectively. The resulting total (applied + induced) field at (to be precise, just outside) the tip of the tube is listed in the table, showing the saturation behavior of the total field when the tube length is beyond $\sim 60\mathring{A}$. We also find that the total field inside the tube is practically zero (see Fig. 5), indicating that the screening of the applied field inside the tube is very effective. Since the discontinuity in the electric field is equal to the surface charge density, the above behavior implies the convergence (saturation) of the induced electronic charge at the tip for the tube length $\gtrsim 60\mathring{A}$. (Even for a tube as short as 36 $\mathring{A}$, the deviation from the converged value is within $\sim$ 25 %.) This behavior is useful for extrapolating to the realistic long-tube-small-field case which is hardly accessible with *ab initio* methods. Another test we have made is that, for a given tube geometry (35 $\mathring{A}$-long FC-CNT), we increase the applied field and obtain the corresponding local field just outside the tip. A linear relation is found as long as the applied field is $\gtrsim$ 0.1 V/$\mathring{A}$. Figure 6 shows such a relation and it may be fit with $E_{tot} = 4.53\ E_{appl} - 0.19$ (V/$\mathring{A}$). The shift (-0.19) is due to the fact that the screening by localized states is not initiated for a small field and the linear increase in the induced field sets off only when the localized states begin to fill. Such a linear relation is again useful for the extrapolation or interpolation purpose. Combining these two results, we can deduce a scaling rule as follows. Since the shift (-0.19 in the above

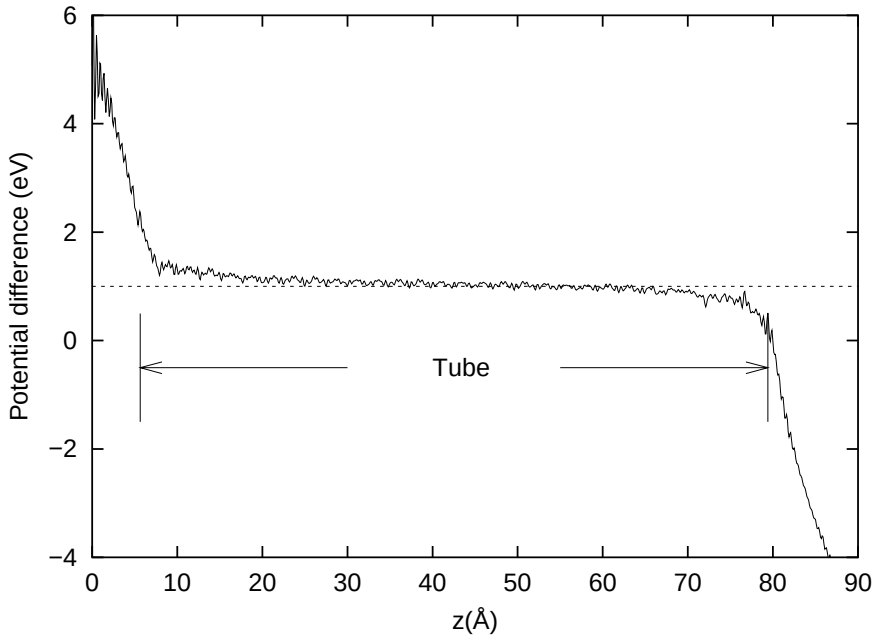

Figure 5. The difference in the total potential when the external field is applied to a 70 $\AA$-CAP-CNT. A horizontal line is drawn for guiding the maintained equipotentiality. The xy coordinate of the plot is set to that of a carbon atom in the top pentagon.

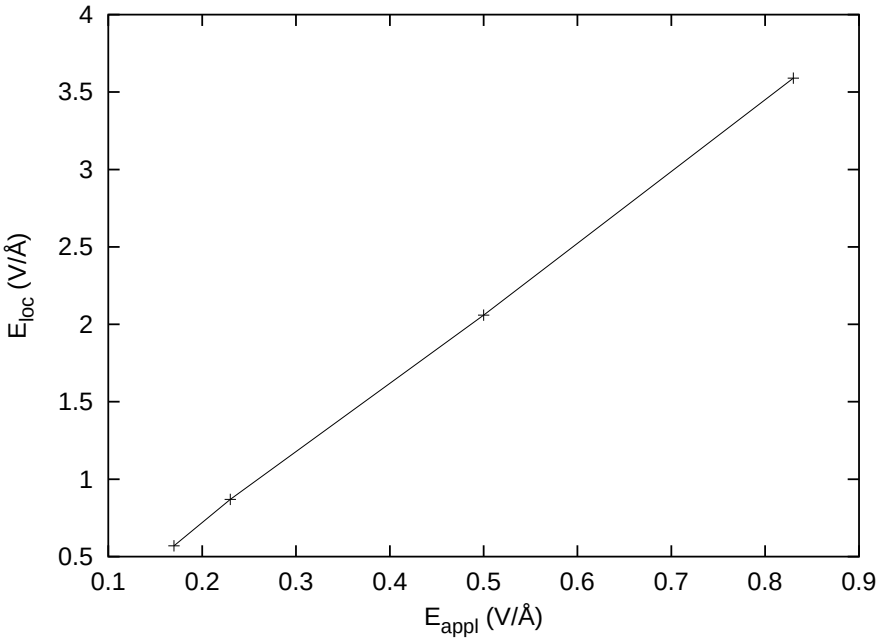

Figure 6. Averaged local field within 3 $\AA$ outside the tip as a function of the applied field for a 35 $\AA$-long FC-CNT. The data are well fit with a straight line.

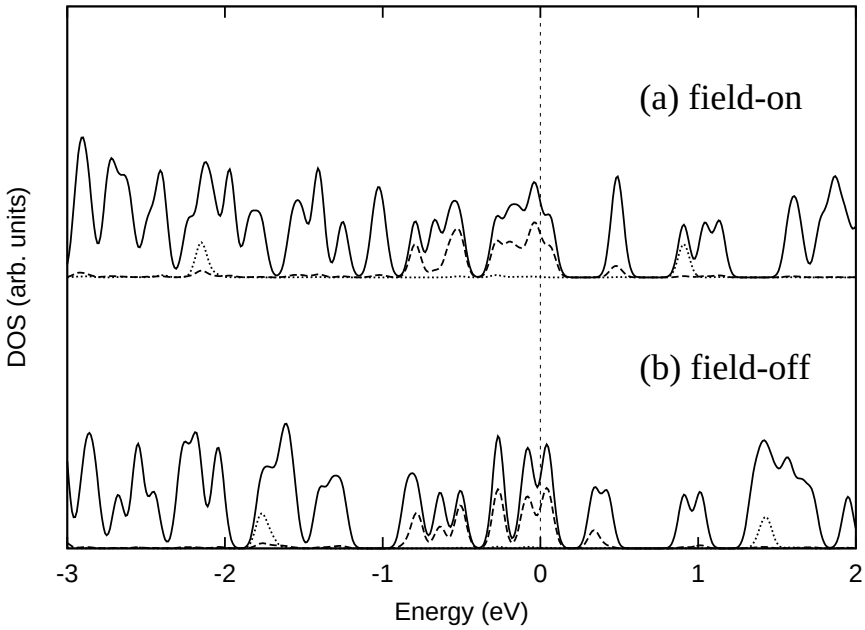

Figure 7. Shift of the localized levels in SC-CNT under the applied field $\sim$0.4 V/$\mathring{A}$. Solid lines are the total DOS. Dashed and dotted lines are the local DOS and they are differentiated as in Fig. 2(d).

case) is generally small, we can approximately express E_{tot} as

$$\mathrm{E}_{tot}(l, \mathrm{E}_{appl}) = a(l) \cdot \mathrm{E}_{appl}, \tag{1}$$

where l is the tube length. On the other hand, we already know that, for a given condition $\mathrm{E}_{appl} \cdot l = c_1$(constant), $\mathrm{E}_{tot}(l, \mathrm{E}_{appl}) \rightarrow c_2$(constant) as l gets large. Therefore, with $\mathrm{E}_{appl} = \dfrac{c_1}{l}$,

$$\mathrm{E}_{tot}(l, \frac{c_1}{l}) = a(l) \cdot \frac{c_1}{l} = c_2, \tag{2}$$

for large l. Then we have $a(l) = \dfrac{c_2}{c_1} l$, namely, $a(l)$ is proportional to l, $\mathrm{E}_{tot} = \alpha l \cdot \mathrm{E}_{appl}$. Using results of independent calculations as well, we obtain that, for a given applied field, the field enhancement factor $\eta (= \mathrm{E}_{tot}/\mathrm{E}_{appl})$ at the edge scales linearly with l,

$$\eta \cong \alpha l \quad . \tag{3}$$

For instance, α of a SC-CNT with the diameter of 7$\mathring{A}$ is approximately 0.17 (with l given in $\mathring{A}$) as will be described below. Equation (1) is distinguished from the result for a conventional metallic prolate spheroid, $\eta \sim m^2/\ln(2m) - 1$ for large m, where m is the aspect ratio, which can be deduced from the depolarization factor[20] of a perfect conductor.

Now we examine the change in the electronic structure by the field in detail. In Fig. 7(a) shown above, the DOS for the SC-CNT under the applied field ($\sim$ 0.4 V/$\mathring{A}$) is plotted. Comparing it with Fig. 7(b) (the same as Fig. 2(d)) for the zero field case, we notice that the localized levels at the armchair edge (dotted curves) undergo a downward shift. The states localized on the zigzag chain sides of the edge are partially occupied for the zero field in Fig. 7(b) (dashed curves) and their occupation increases

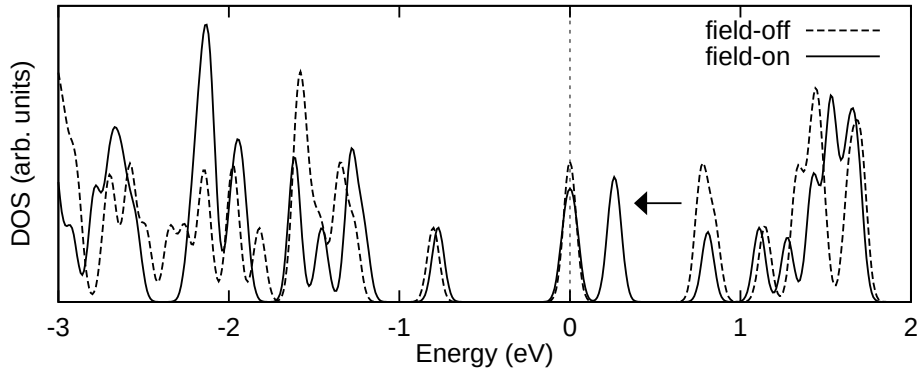

Figure 8. Shift of the localized levels in CAP-CNT. Note that other π states are not much changed.

as the field is turned on. Such a situation is commonly observed in the field emission of metallic tips with atomic adsorbates[21]. Since these states are located at the Fermi level under the applied field, they are the first to be emitted across the barrier to the anode. The increase in the occupation of the dangling bond states is approximately $0.1e$ per edge atom. The downward shift of the localized states by the field occurs in the FC-CNT and CAP-CNT as well. (See Fig. 8 for the case of the CAP-CNT.) Shifts of the localized states are pinned as they begin to be occupied, hence these localized states stay at the Fermi level for a wide range of the field strength. The occupation of the localized states has an effect of repulsing the π-electrons and suppresses the increase in the amplitude of the π states at the edge. Actually, the sum of the accumulated charge does not vary too much from structure to structure.

LOCAL FIELD ENHANCEMENT

The accumulated charge at the end of the CNT as described above enhances the local electric field, which is the driving force of the field emission. For a quantitative analysis, we calculate the *change* in the charge density under the applied field of 0.17 V/$\mathring{A}$ using the *ab initio* method with localized orbitals and plot the resulting Coulomb potential for an isolated tube along the tube axis in Fig. 9. The down slope on the left of the peak is essentially the negative of the applied field which screens out the applied field inside the tube. The down slope on the right of the peak, on the other hand, is the induced field that reduces the potential barrier when electrons are emitted across the vacuum barrier to the anode side. The difference between the H-CNT and other systems can be considered as contributions from the localized states inherent to the tip structures in Fig. 1(b)-(d).

A striking feature in Fig. 9 is the prominent potential peak and the corresponding high field enhancement of the SC-CNT among the model systems. The average induced fields within 3 $\mathring{A}$ from the peak position to the right (vacuum region) are 0.53, 0.58, 0.65, and 1.03 V/$\mathring{A}$ for (a)-(d) geometries, respectively. The aforementioned extrapolations to a realistic 2 μm-long tube lead to the field enhancement factors of 1700, 1900, 2100, and 3300, respectively, which compare favorably with the experimental values of 3600[2] or 1300[4]. A greater enhancement factor of the SC-CNT than the CAP-CNT is consistent with experiment[5] considering that the multiwall open CNT used in experiment should have some unsaturated dangling bonds like the SC-CNT studied

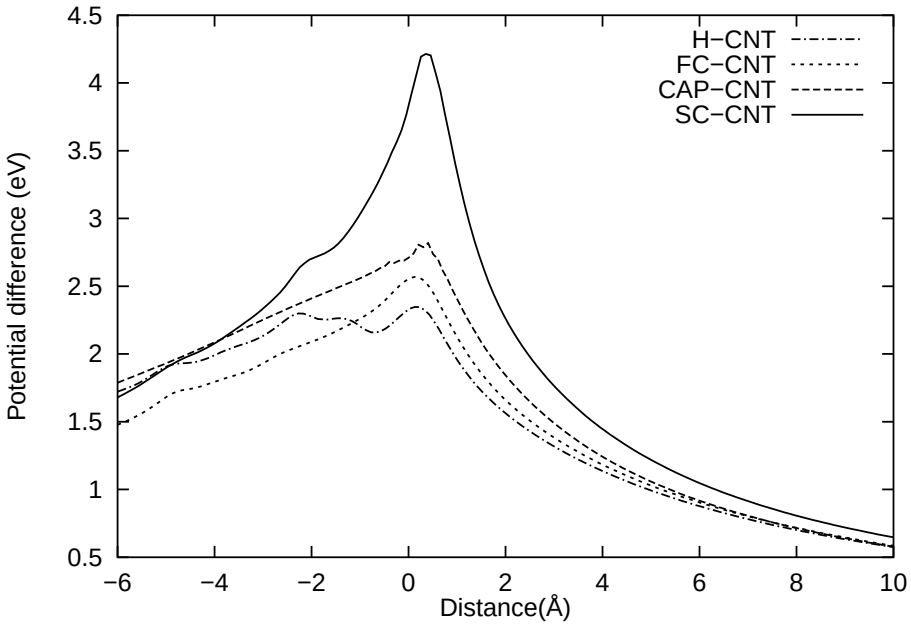

Figure 9. Coulomb potential generated by the induced charge and plotted in the tube axis direction when the external field of 0.17 V/$\mathring{A}$ is applied for $\sim$ 35 $\mathring{A}$-long tubes. The distance is measured from the edge of the tube.

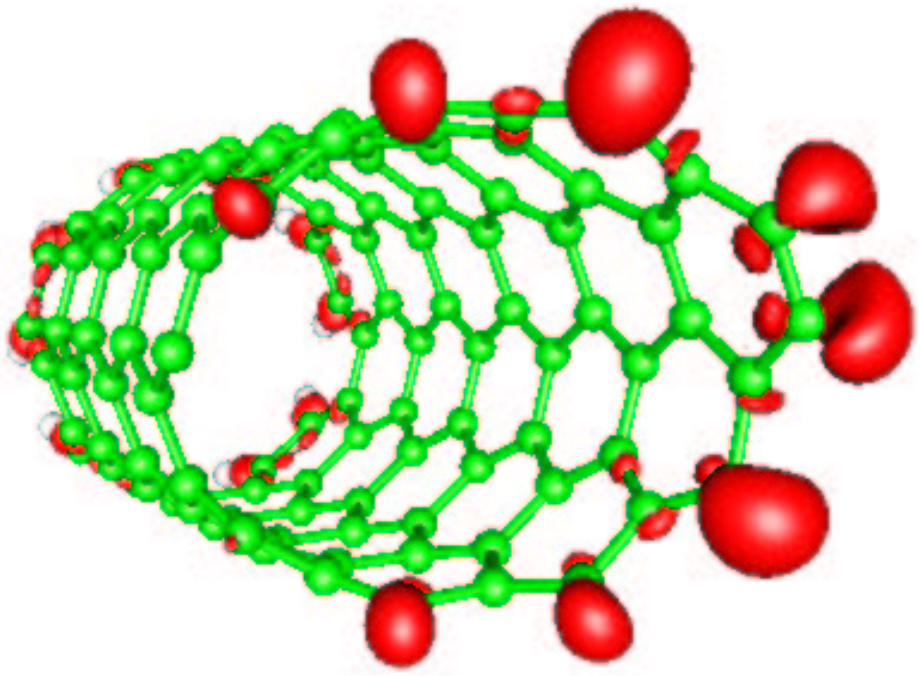

Figure 10. Perspective view of the constant density (0.01 $e/\mathring{A}^3$) surface showing the density *change* in the SC-CNT under the external field of 0.4 V/$\mathring{A}$. The σ-bond-derived character is clearly visible.

here. One might expect that the highest induced field in the SC-CNT should originate from its sharpest armchair edge (hence the highest field enhancement factor according to classical electrostatics) among the studied structures. However, when we probe the induced electric field very closely all over the space, we find that the region around the zigzag side edge has a field at least as large as that of the topmost atoms. To identify the origin of the high field unambiguously, we have performed the same calculation for a flat-cut (12,0) zigzag-type nanotube. We find a sharp Coulomb potential peak identical to the SC-CNT. We conclude that the unpaired dangling-bond states at the Fermi level under the applied field, which exist both in the SC-(n,n) CNT and the FC-(3n,0) CNT, are mainly responsible for the highest potential peak, i.e., the largest induced field toward the anode side. Therefore, the most favorable tip geometry for the field emission in our study is the open tube with the zigzag-type edge where unsaturated dangling bond states can exist. In Fig. 10, we show an isodensity surface of the induced charge accumulated at the end of the SC-CNT in the presence of the applied field of 0.4 V/$\mathring{A}$. The plot exhibits dangling bond states as expected from the above analysis. We also emphasize that the lobes of these dangling bond wave functions are directed toward the anode side and their overlap integral with the tail of the free-electron-like state from the anode side of the barrier is relatively large (meaning a large emission probability), while the π-electron states on the tube body lie perpendicular to the emission direction and the corresponding overlap integral is much smaller.

It is interesting that the CAP-CNT has the next highest peak in Fig. 9, higher than that of the FC-CNT. The occupation of the π states in the hemispherical region of the CAP-CNT easily increases as the external field is turned on and contributes to the induced field efficiently because they are at the Fermi level. These π-electrons are the first to be emitted under the applied field for the CAP-CNT. Since the π-electron at the top of the hemisphere points to the anode side, the overlap integral mentioned above is reasonably large in this case. We also note that, although the H-CNT has a relatively small induced Coulomb potential, its magnitude is still appreciable in Fig. 9. The accumulated charge here is the usual metallic π states of the tube whose amplitude has increased at the edge to screen the applied field as in typical metallic samples. Our results show that both the localized states and the metallic π states can contribute to the field enhancement. To see the contributions of the two separately in the SC-CNT, we attach H atoms to the dangling bonds in the SC-CNT (not shown). We find that the passivation of the dangling bonds quenches the field enhancement to the level of the H-CNT.

We have also studied the effects of the image potential for the H-CNT and CAP-CNT by artificially putting an electron represented by $1/r$ potential to a point in the hypothetical tunneling trajectory. The image potential is calculated from the change in the self-consistent potential at that point. The result is shown in Fig. 11 and the data set obtained in this way are fitted with the classical form of the image potential for an infinite metal plane, $-\alpha\dfrac{e}{4(z-z_0)}$. The fitted α and z_0 are shown in Table 1. Since the geometry of the CNT is cylindrical rather than flat, the distance between the image charge generated on the CNT and the displaced electron would be effectively greater than those in the flat metal surface. The deeper potential for the CAP-CNT comes from the existence of the cap perpendicular to the z-axis where large amount of positive charge could gather close to the displaced electron. Another physical quantity crucial to the current profile in the field emission is the work function of the nanotube. We find that the calculated work function of the isolated CNT ($\gtrsim$ 4 eV, which is not fully converged in our finite unit cell calculation, but still reasonably close to experimental values of 4.5 - 5.3 eV[2,23,24]) is insensitive to the tip geometry, giving small variations

within 0.1 eV.

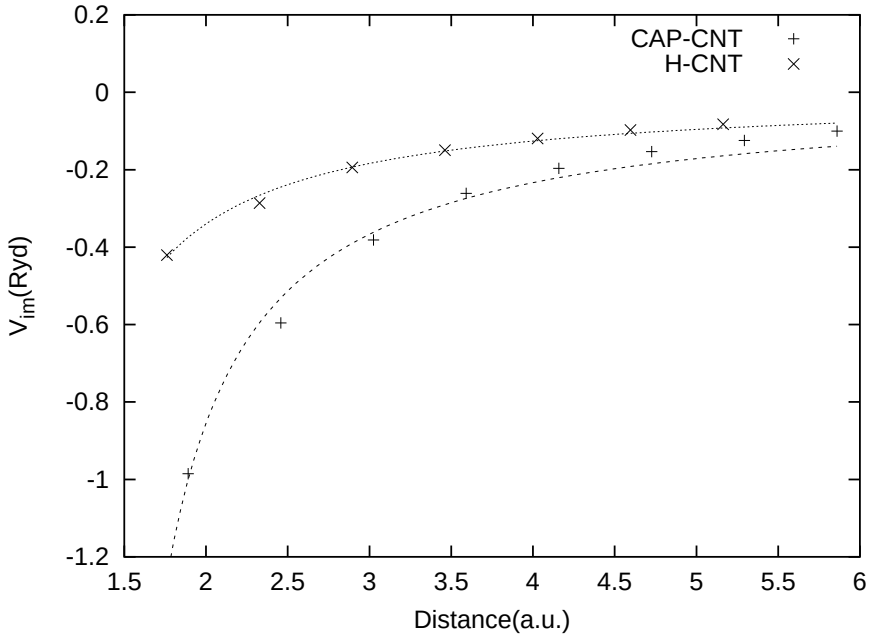

Figure 11. Image potential for the H-CNT and CAP-CNT. The origin of the z-axis is set to the position of the outermost atom for each system. The curves are the best fit of the function $-\alpha e/4(z-z_0)$ to the data points.

	α	z_0
H-CNT	0.64	1.25
CAP-CNT	0.4	0.82
metal plane	1	0.0

Table 1. The fitted parameters of the curves in Fig. 11.

Field Emitter Array

Another interesting issue we pursue here is the dependence of the field enhancement factor on the separation and packing of the nanotubes. We have already presented the results for an isolated nanotube and now show other cases. We have performed the same electronic structure calculations with the rope (infinite hexagonal array of nanotubes in the xy plane separated by 3.4 $\mathring{A}$ from each other with a finite length in z direction). The self-consistent electronic structures with and without the applied electric field are calculated and the induced charge is obtained. Then we calculate the field at the tube edge produced by an isolated tube with this induced charge, that produced by a (3×3) array of tubes (at the edge of the central tube), that by a (5×5) array of tubes, etc. Figure 12 shows the field obtained in this way and this plot implies two crucial effects. First, as the number of close-packed nanotubes increases, the field decreases. This is expected because the larger the packed area is, the more similar to the planar geometry (which does not enhance the field) is the configuration. The effective curvature of the tube at the edge is substantially reduced when the tubes form a rope. The converged value of E_{ind} in the large n limit here is only about a quarter of the field produced by a tube in the isolated configuration studied above. Secondly,

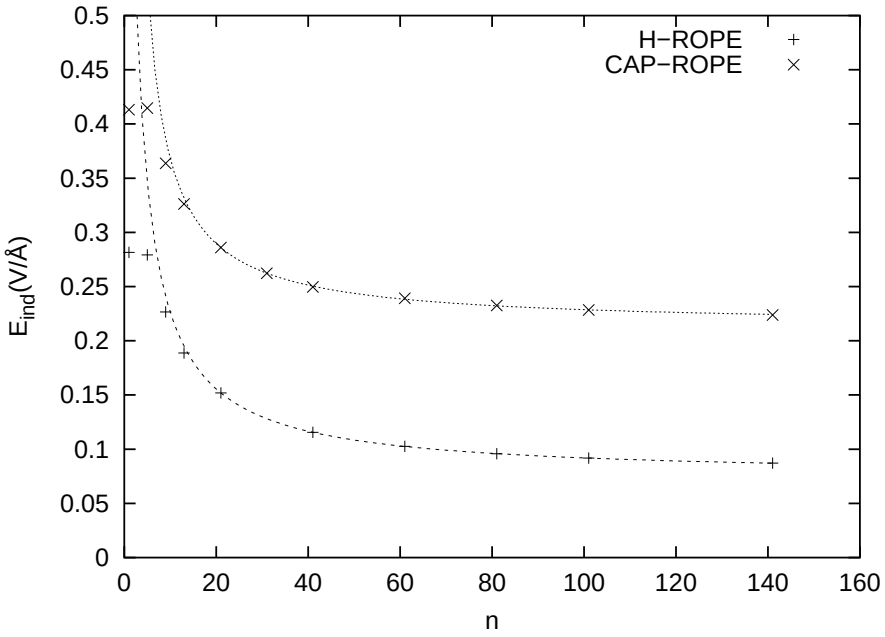

Figure 12. The induced field at the edge of the central tube in a rope. The abscissa is the number of close-packed tubes along a side of square that contribute to the field of the central tube. The asymptotic behavior is nicely fitted with the curve $a/(n-b)+c$.

the induced charge per tube in the rope configuration is also significantly diminished compared with that in the isolated case. The field for $n = 1$ in Fig. 12 is only about half of the corresponding field produced by the isolated tube under the some applied field. Therefore it is desirable to deposit (or grow) nanotubes far apart from each other for efficient field emission. The enhancement is effective if the separation between tubes is beyond a few nanometers. Another desirable, yet difficult thing to achieve is to have singlewall nanotubes rather than multiwall tubes. It is also found that the ratio of E_{ind} between CAP-CNT and H-CNT is significantly enlarged from that in the isolated situation, which implies that the effects of localized states and the shape of the end structure become more important in the close-packed configuration.

DISCUSSION

In summary, we have studied the electronic structure of various edge shapes of a singlewall nanotube with or without external fields. A linear scaling behavior of the field enhancement factor as a function of the tube length has been obtained. Open tubes with dangling bonds at the zigzag-type edge are predicted to be the most favorable for the field emission among the structures considered here. The capped nanotubes with π-bonding states localized at the cap region are the next favorable structure. In a real situation, it is likely that hydrogen atoms or other ambient atoms and molecules cap the reactive dangling bonds of the open nanotubes. However, the attached atoms or molecules may be desorbed by an initial clean-up procedure before emission or by a strong local field during the emission process. Fortunately, the strong sp^2 bond of the tube body is not dissociated at all under the typical field ($\lesssim 1$ V/$\mathring{A}$) in experiment. For multiwall CNT cases, the saturated (3-fold) coordination of all edge atoms by bridging carbon atoms cannot occur in general because of the the incommensurability between neighboring coaxial tubes, and there should remain some unsaturated dangling bonds

contributing actively to the field emission[22]. Existing experimental data do not yet give information on the dependence of the emission efficiency on the tip structure. Our study proposes a high-efficiency edge structure which can significantly improve the field emission performance. We also note that, for the practical display application, it is enough for only a small fraction of nanotubes to actually emit electrons because of huge redundancy in the total number of nanotube emitters.

Acknowledgment. - The study on the carbon nanotube field emitter array was supported by the Samsung Electronics. This work was supported by the BK21 Project of the MOE, the SRC Program of the KOSEF, and the BSRI Program of the KRF.

REFERENCES

1. Y. Saito, K. Hamaguchi, T. Nishino, K. Hata, K. Tohji, A. Kasuya, and Y. Nishina, Jpn. J. Appl. Phys. **36**, L1340 (1997).
2. J.-M. Bonard, J.-P. Salvetat, T. Stockli, W. A. de Heer, Appl. Phys. Lett. **73**, 918 (1998).
3. A. G. Rinzler, J. H. Hafner, P. Nikolaev, L. Lou, S. G. Kim, D. Tomanek, P. Nordlander, D. T. Colbert, and R. E. Smalley, Science **269**, 1550 (1995)
4. W. A. de Heer, A. Chatelain, and D. Ugarte, Science **270**, 1179 (1995).
5. Y. Saito, K. Hamaguchi, S. Uemura, K. Uchida, Y. Tasaka, F. Ikazaki, M. Yumura, A. Kasuya, and Y. Nishina, Appl. Phys. A **67**, 95 (1998).
6. Q. H. Wang, T. D. Corrigan, J. Y. Dai, and R. P. H. Chang, Appl. Phys. Lett. **70** 3308 (1997).
7. P. G. Collins and A. Zettl, Appl. Phys. Lett. **69**, 1969 (1996); P. G. Collins and A. Zettl, Phys. Rev. B **55**, 9391 (1997).
8. Q. H. Wang, A. A. Setlur, J. M. Lauerhaas, J. Y. Dai, E. W. Seelig, and R. P. H. Chang, Appl. Phys. Lett. **72**, 2912 (1998); Y. Saito, S. Uemura, and K. Hamaguchi, Jpn. J. Appl. Phys. **37**, L346 (1998); W. B. Choi, D. S. Chung, S. H. Park, and J. M. Kim, in Proceedings of the MRS Spring Meeting, San Francisco (1999) (unpublished).
9. Z. F. Ren, Z. P. Huang, J. W. Xu, J. H. Wang, P. Bush, M. P. Siegal, and P. N. Provencio, Science **282**, 1105 (1998); S. Fan, M. G. Chapline, N. R. Franklin, T. W. Tombler, A. M. Cassell, and H. Dai, *ibid.* **283**, 512 (1999).
10. S. Fan, M. G. Chapline, N. R. Franklin, T. W. Tombler, A. M. Cassell, and H. Dai, Science **283**, 512 (1999).
11. J. Ihm, A. Zunger and M. L. Cohen, J. Phys. C:Solid State Phys., **12**, 4409 (1979).
12. N. Troullier and J. L. Martins, Phys. Rev. B **43**, 1993 (1991).
13. Seungwu Han and Jisoon Ihm (to be published).
14. O. F. Sankey and D. J. Niklewski, Phys. Rev. B **40**, 3979 (1989); The r_C is set to 4.0 for C and H atoms.
15. C. H. Xu, C. Z. Wang, C. T. Chan, and K. M. Ho, J. Phys.: Condens. Matter **4**, 6047 (1992).
16. D. L. Carroll, P. Redlich, P. M. Ajayan, J. C. Charlier, X. Blase, A. De Vita, and R. Car, Phys. Rev. Lett. **78**, 2811 (1997).
17. P. Kim, T. W. Odom, J.-L. Huang, and C. M. Lieber, Phys. Rev. Lett. **82**, 1225 (1999); R. Tamura and M. Tsukada, Phys. Rev. B **52**, 6015 (1995).
18. A. De Vita, J. -Ch. Charlier, X. Blase, and R. Car, Appl. Phys. A **68**, 283

(1999).
19. M. Fujita, K. Wakabayashi, K. Nakada, and K. Kusakabe, J. Phys. Soc. Japan. **65**, 1920 (1996).
20. J. A. Osborn, Phys. Rev. **67**, 351 (1945).
21. V. T. Binh, S. T. Purcell, N. Garcia, and J. Doglioni, Phys. Rev. Lett. **69**, 2527 (1992); M. L. Yu, N. D. Lang, B. W. Hussey, T. H. P. Chang, and W. A. Mackie, Phys. Rev. Lett. **77**, 1636 (1996).
22. J. Charlier, A. De Vita, X. Blase and R. Car, Science **275**, 646 (1997).
23. O. M. Kuttel, O. Groening, C. Emmenegger, and L. Schlapbach, Appl. Phys. Lett. **73**, 2113 (1998).
24. S. J. Tans, A. R. M. Verschueren, and C. Dekker, Nature **393**, 49 (1998).